

A POWER FLOW METHOD FOR EVALUATING VIBRATION FROM UNDERGROUND RAILWAYS

M.F.M. Hussein, H.E.M. Hunt

*Engineering Department, Cambridge University, Trumpington Street, Cambridge, CB2 1PZ, UK.
Tel: +44 1223 765925, Fax: +44 1223 332662, E-mail: mfmh2@cam.ac.uk, hemh@cam.ac.uk*

Abstract

One of the major sources of ground-borne vibration is the running of trains in underground railway tunnels. Vibration is generated at the wheel–rail interface from where it propagates through the tunnel and surrounding soil into nearby buildings. An understanding of the dynamic interfaces between track, tunnel and soil is essential before engineering solutions to the vibration problem can be found.

A new method has been developed to evaluate the effectiveness of vibration countermeasures. The method is based on calculating the mean power flow from the tunnel, paying attention to that part of the power, which radiates upwards to places where buildings' foundations are expected to be found. The mean power is calculated for an infinite train moving through the tunnel with a constant velocity. An elegant mathematical expression for the mean power flow is derived, which can be used with any underground-tunnel model.

To evaluate the effect of vibration countermeasures and track properties on power flow, a comprehensive three-dimensional analytical model is used. It consists of Euler-Bernoulli beams to account for the rails and the track slab. These are coupled in the wavenumber–frequency domain to a thin shell representing the tunnel embedded within an infinite continuum with a cylindrical cavity representing the surrounding soil.

1. Introduction

Underground railways are important for solving traffic congestion in densely populated cities. A serious disadvantage is the vibration generated by trains, which propagates from the wheel–rail interface through the tunnel and surrounding soil into nearby buildings. Many methods are used to decrease vibration levels in nearby structures. One of the most effective methods is to isolate vibration at the source. A good example of source isolation is the use of floating-slab track as

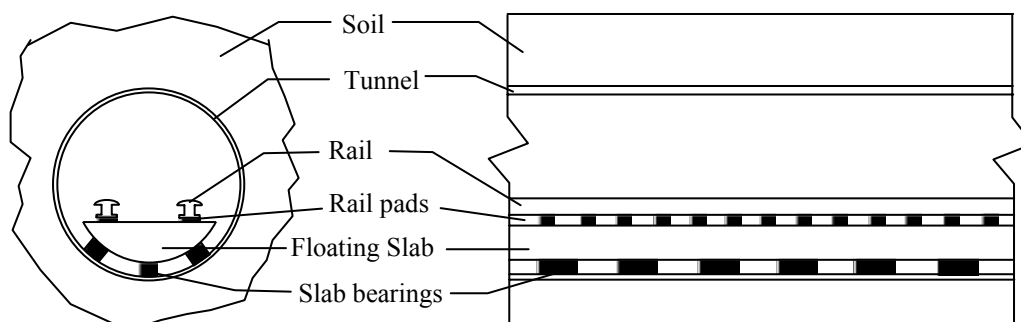


Figure 1: Layout of an underground-tunnel showing the different structural components (in this figure the floating slab is mounted on three lines of discrete slab-bearings).

illustrated in Figure 1. The principal components relevant to vibration modelling are the rails, the railpads and the floating slab. The floating slab is coupled via slab bearings to the tunnel wall, which lines a cavity in the soil.

This paper presents a new method to evaluate the effect of vibration countermeasures based on mean power flow calculations. A detailed description of the method is given in section 2. Section 3 and 4 discuss the tunnel–soil model and the track model respectively. Section 5 discusses the calculation procedure and finally by means of a parametric survey section 6 provides some insight into behaviour of the model and the effect of track properties on mean power flow.

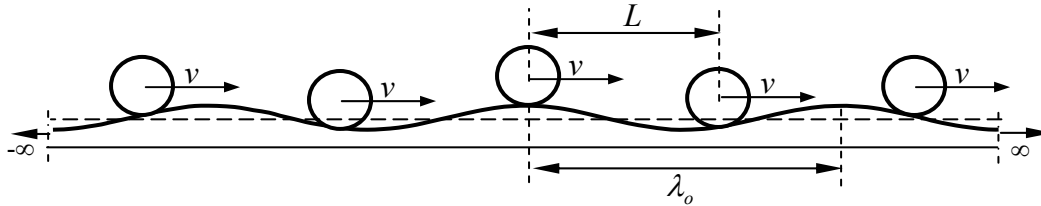


Figure 2: Infinite number of masses moves over a rail with roughness of wavelength λ_0 and magnitude Δ_o . Rail displacements are not shown.

2. Mean power flow due to an infinite moving-train

A set of moving axles, infinite in number and with fixed axle spacing L , is used to model a train moving in an underground tunnel. The train model is shown in Figure 2, where only unsprung masses are considered to give rise to dynamic forces on the track. The train moves with velocity v and due to a given sinusoidal rail roughness of wavelength λ_0 , the rail experiences a harmonic excitation with angular frequency $\varpi = 2\pi v / \lambda_0$.

In this paper correlated roughness on the two rails is assumed. Thus the beam in Figure 2 represents both rails of the track. The derivation in this section has been extended to uncorrelated roughness and soon to be published. This section is divided into three parts: firstly expression is found for the displacement at any point in the track or soil, secondly the velocity and stress expressions are calculated, and finally these expressions are used to calculate the mean power flow.

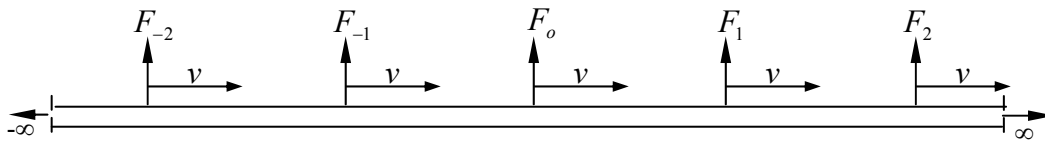


Figure 3: Loading on the rail equivalent to the one in Figure 2. $F_k = G \cdot e^{i\varpi t} e^{ik\varpi L / v}$.

2.1 Displacement calculation

The loading in Figure 2 is dynamically equivalent to a set of oscillating moving loads $F_k = G \cdot e^{i\varpi t} e^{ik\varpi L / v}$ as shown in Figure 3. G is the magnitude of the applied force (constant for all axles), the phase difference between any adjacent loads is $\varpi L / v$, and the index k varies from $-\infty$ to ∞ . The load on the rail can be written in a continuous form as

$$F(x, t) = \sum_{k=-\infty}^{\infty} G \cdot e^{i\varpi t} e^{ik\varpi L/v} \cdot \delta(x - vt - kL). \quad (1)$$

This force is transformed to the wavenumber–frequency domain $\xi - \omega$ using the double Fourier transform in time and space [1] to give

$$\tilde{F}(\xi, \omega) = 2\pi \sum_{k=-\infty}^{\infty} G \cdot e^{-i\xi nL} e^{ik\varpi L/v} \cdot \delta(\omega + \xi v - \varpi). \quad (2)$$

The displacement of the track or soil due to this loading is calculated using the convolution integral [1] as a multiplication in the $\xi - \omega$ domain. Hence

$$\tilde{Y}(\xi, \omega) = 2\pi \cdot \tilde{H}(\xi, \omega) \cdot \sum_{k=-\infty}^{\infty} G \cdot e^{-i\xi kL} e^{ik\varpi L/v} \cdot \delta(\omega + \xi v - \varpi) \quad (3)$$

where $\tilde{H}(\xi, \omega)$ is the displacement frequency response function (FRF), *i.e.* the displacement of the measuring point (at track or soil) in the wavenumber–frequency domain for a unit force at the rail in the same domain. Transforming back to the time domain gives

$$\tilde{Y}(\xi, t) = \tilde{H}(\xi, \varpi - \xi v) \cdot G \cdot e^{i(\varpi - \xi v)t} \sum_{k=-\infty}^{\infty} e^{ikL(\varpi/v - \xi)}. \quad (4)$$

The infinite sum of exponential functions can be written as an equivalent sum of delta functions [1] to give

$$\tilde{Y}(\xi, t) = \tilde{H}(\xi, \varpi - \xi v) \cdot G \cdot e^{i(\varpi - \xi v)t} \cdot \frac{2\pi}{L} \sum_{k=-\infty}^{\infty} \delta(\xi - \varpi/v + \frac{2\pi k}{L}) \quad (5)$$

where k no longer gives the load index. Transforming back to the space domain and rearranging gives

$$y(x, t) = \sum_{k=-\infty}^{\infty} e^{i\xi_k x} e^{i\omega_k t} \left[\frac{G \cdot \tilde{H}(\xi_k, \omega_k)}{L} \right] \quad (6)$$

where

$$\xi_k = \frac{\varpi}{v} - \frac{2\pi k}{L} \quad \text{and} \quad \omega_k = \frac{2\pi k v}{L}.$$

This important result gives the displacement at any point in the track – soil system. It expresses the displacement as a sum of infinite convecting waves. Each wave is described with its angular frequency ω_k and wavenumber ξ_k , which is called the *wavenumber deficit*.

2.2 Velocity and stress calculations

Before writing the velocity and stress expressions, the magnitude of the force amplitude G in (6) is calculated by comparing the loading in Figure 2 and 3 and writing the equilibrium of the mass located at $x = 0$ at time $t = 0$. This results in

$$G = \frac{M \cdot \Delta_o \cdot \varpi^2}{1 - y(0,0)|_{G=1} \cdot M \cdot \varpi^2} \quad (7)$$

where M is the unsprung mass and Δ_o is the roughness amplitude.

One can now calculate the velocity and stress at a point in soil by substituting the velocity and stress FRFs ($\tilde{V}(\xi_k, \omega_k)$ and $\tilde{\tau}(\xi_k, \omega_k)$) for the displacement FRF $\tilde{H}(\xi, \omega)$ in (6) to give

$$V(x, t) = \sum_{k=-\infty}^{\infty} e^{i\xi_k x} e^{i\omega_k t} \left[\frac{G \cdot \tilde{V}(\xi_k, \omega_k)}{L} \right] \quad (8)$$

$$\tau(x, t) = \sum_{k=-\infty}^{\infty} e^{i\xi_k x} e^{i\omega_k t} \left[\frac{G \cdot \tilde{\tau}(\xi_k, \omega_k)}{L} \right]. \quad (9)$$

2.3 Mean power calculation

Instantaneous local power flow is the product of local velocity and local stress. This forms the basis of mean power flow method. The mean power flow can be calculated as

$$P(x) = \frac{v}{L} \int_{t=0}^{t=L/v} \text{Re}(V(x, t)) \cdot \text{Re}(\tau(x, t)) \cdot dt. \quad (10)$$

Substituting (8) and (9) into (10), after simplifications results in

$$P(x) = \frac{|G|^2}{2L^2} \sum_{k=-\infty}^{\infty} \text{Re}[\tilde{V}(\xi_k, \omega_k) \cdot \tilde{\tau}^*(\xi_k, \omega_k)] \quad (11)$$

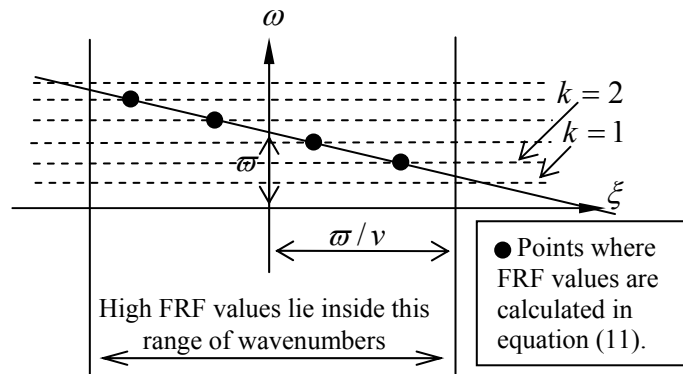


Figure 4: Demonstration of the wavenumber region used in calculating (11).

where $()^*$ denotes the conjugate of the complex quantity. The significance of this result is that it is independent of the longitudinal coordinate x . This confines the problem to the two-dimensional plane perpendicular to the longitudinal direction.

The infinite sum in (11) can be approximated as a finite sum performed over the region with large FRF response. This is made clear in Figure 4 where the significant values of wavenumber deficit ξ_k are those that map onto regions of high $\tilde{V}(\xi, \omega)$ and $\tilde{\tau}(\xi_k, \omega_k)$.

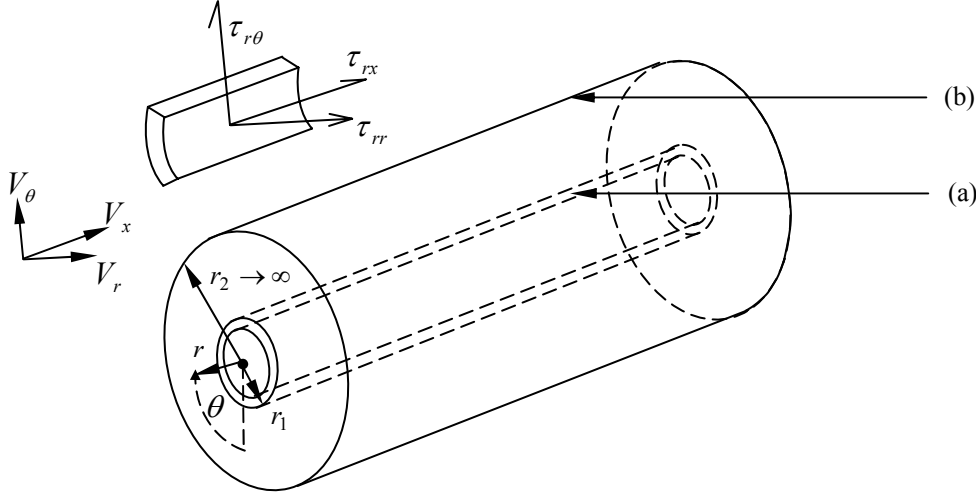


Figure 5: Tunnel wall and soil models: (a) tunnel wall of outer radius r_1 modelled as a thin cylindrical shell of infinite length. (b) Surrounding soil modelled as an infinite domain with cylindrical cavity.

3. Tunnel and soil model

A three-dimensional model for an underground tunnel and the surrounding soil is introduced by Forrest [2]. The tunnel wall is modelled as a thin cylindrical shell, while the soil around the tunnel is modelled using elastic continuum theory as an infinite domain containing a cylindrical cavity as shown in Figure 5.

The time-varying distributed stress applied to the tunnel wall is denoted $\tau(x, \theta, t)$, where x is the distance measured along the tunnel and θ is the angle measured around the circumference. This stress is transformed to the wavenumber domain using the Fourier transform along the direction x and due to circular periodicity, the θ dimension is decomposed into a discrete Fourier series with symmetrical and anti-symmetrical components at the tunnel wall. The form of loading with symmetrical components with respect to θ can be written as

$$\tau(x, \theta, t) = \begin{bmatrix} \tilde{\tau}_{rx} \cos n\theta \\ \tilde{\tau}_{r\theta} \sin n\theta \\ \tilde{\tau}_{rr} \cos n\theta \end{bmatrix}_{r=r_1} e^{i(\omega t + \xi x)} \quad (12)$$

where r_1 is the internal radius of the tunnel. Note in (12) that $\tilde{\tau}_{r\theta} \sin n\theta$ is symmetrical rather than anti-symmetrical due to the sign convention for stress components as shown in Figure 5. The soil velocities at radius r_0 measured from the tunnel centre, for the stress in (12), can be written as

$$V(x, \theta, t) = \begin{bmatrix} \tilde{V}_x \cos n\theta \\ \tilde{V}_\theta \sin n\theta \\ \tilde{V}_r \cos n\theta \end{bmatrix}_{r=r_o} e^{i(\omega t + \xi x)}. \quad (13)$$

To account for anti-symmetrical components (for instance when torsional loading of the slab is considered), equations (12) and (13) are used again but every $\cos n\theta$ should be changed to $\sin n\theta$ and vice versa. When coupling a track to this model, the circumferential distribution of forces on tunnel wall depends on connectivity of track. The model response to symmetrical and anti-symmetrical components can be found and the total response is calculated by adding the individual responses from (13). More details about the model are found in [2].

4. The track model

The track model consists of two rails and a main track slab modelled as Euler-Bernoulli beams. Rails transmit the load to the slab through railpads. Railpads are modelled as continuous resilient layers under the rails. The track is supported on the tunnel wall via slab bearings. Only bending of slab is considered. The inclusion of torsional effects is straightforward but not presented here. Three kinds of slab supports are considered as shown in Figure 6. The slab bearings in these models are continuous in the longitudinal direction and have both normal and shear stiffness. The main track slab is identified by its natural frequency. This is defined as the vertical cut-on frequency of the slab supported on a rigid tunnel via these slab bearings. The natural frequency of each slab can be calculated from the relationships in (14) to (16) for three cases (a), (b), and (c):

(a) for two lines of support as in Figure 6.a

$$f_n = \frac{1}{2\pi} \sqrt{\frac{k_n (2 \cos^2 \Omega + 2\mathfrak{R} \cdot \sin^2 \Omega)}{m_s}}; \quad (14)$$

(b) for three lines of support as in Figure 6.b

$$f_n = \frac{1}{2\pi} \sqrt{\frac{k_n (2 \cos^2 \psi + 1 + 2\mathfrak{R} \sin^2 \psi)}{m_s}}; \quad (15)$$

(c) for uniform support as in Figure 6.c

$$f_n = \frac{1}{2\pi} \sqrt{\frac{r_t k_n [\phi(1 + \mathfrak{R}) + 0.5(1 - \mathfrak{R}) \sin 2\phi]}{m_s}} \quad (16)$$

where k_n is the slab-bearing normal stiffness, \mathfrak{R} is the ratio between the shear to the normal stiffness, *i.e.* $\mathfrak{R} = k_s / k_n$, k_s is the slab-bearing shear stiffness, m_s is the slab mass per unit length,

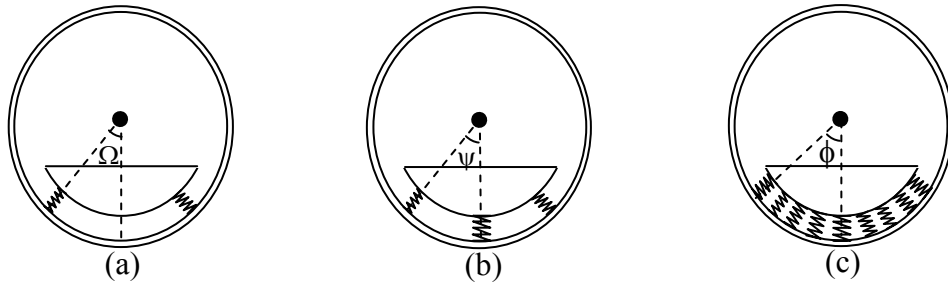


Figure 6: Coupling of the slab to the tunnel–soil model via: (a) two lines, (b) three lines, and (c) uniform continuous support. Rails are not shown in the figure.

r_i is the inner radius of the tunnel, and Ω , ψ , and ϕ are the angles of bearings distribution and are shown in Figure 6.

The main track slab is modelled in two ways, either “direct fixation” or “floating”. “Direct fixation” is modelled as case (c) (uniform support) by setting the slab-bearing stiffness to infinity. “Floating” track is modelled with any of the cases in Figure 6 according to distribution of slab bearings.

The track models are coupled to the tunnel–soil model in the wavenumber–frequency domain. This is done by considering equilibrium of forces and displacement at the interface between slab bearings and the tunnel wall. This allows for calculation of the velocity and stress FRFs at any given point (r, θ) in the soil for a unit input at the rails in the wavenumber–frequency domain.

5. Power calculation

The region of most interest for vibration in buildings is that part of the soil above the tunnel since this is where foundations of buildings are located. Power radiated downwards is generally of no interest except perhaps in the case of rigid bedrock, not considered here. Hence the mean power radiated upwards from the tunnel (see Figure 7) is calculated and for the best design of track this value should be minimized. The power radiated through a circular sector with radius r_o and bounded by the two angles θ_1 and θ_2 can be calculated from the following expressions

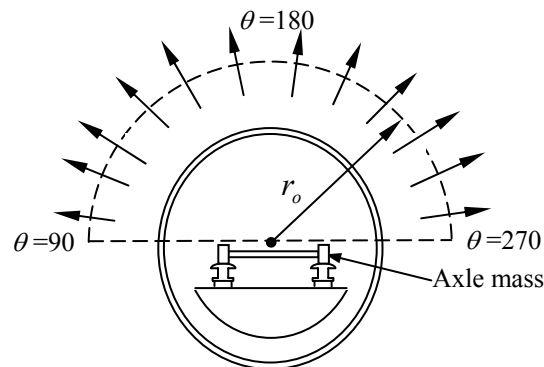


Figure 7: Mean power flow radiated upward calculated at distance r_o from the tunnel center due to infinite number of axles moving on the rails. Slab bearings are not shown in the diagram.

$$P(\theta_1, \theta_2) = \frac{|G|^2}{2L^2} \int_{\theta_1}^{\theta_2} \sum_{k=-\infty}^{\infty} \text{Re}[\tilde{V}_x(\xi_k, \omega_k) \cdot \tilde{\tau}_{rx}^*(\xi_k, \omega_k) + \tilde{V}_\theta(\xi_k, \omega_k) \cdot \tilde{\tau}_{r\theta}^*(\xi_k, \omega_k) + \tilde{V}_r(\xi_k, \omega_k) \cdot \tilde{\tau}_{rr}^*(\xi_k, \omega_k)] r_o d\theta \quad (17)$$

The three components in this expression take account of the power contributions from the longitudinal, tangential, and radial stresses respectively. This method provides an effective tool for checking the calculated expressions for stresses and displacements in the soil. The mean power calculated in this way for all closed boundaries that enclose the tunnel wall are identical as there are no internal sources of power in the soil and no losses for the case of zero soil damping. The power radiated upwards can be evaluated using a semicircular boundary of radius r_o as shown in Figure 7. For the parameters given section 6, it is found that the evaluated mean power is effectively invariant for values of $r_o \geq 10m$ because there is no significant change of power flow across the horizontal part of the boundary. Below this radius, it becomes necessary to account for power flow through the horizontal part of the boundary.

6. Effect of track properties on power flow

In this section, the general features of mean power flow from an underground tunnel are investigated. Hence the effects of changing parameters such as unsprung mass, bending stiffness of rail and slab, stiffness of railpads and slab bearings, and the distribution of slab bearings are studied.

Figure 8(a, b) show the magnitude of the tangential and radial velocity FRFs at $\theta=90^\circ$ and 180° respectively at radius $r_o=10m$ for a 20Hz slab on uniform support. The distinct white curves indicate high values of the velocity FRF and two continuous curves are clearly visible. These correspond to the *propagation curves* for a track on a rigid foundation as confirmed later (Figure 11.b). The propagation curve is used to determine the wavenumber of free wave propagation at a given frequency. Dispersion curves can be obtained by plotting wavenumber divided by the angular frequency versus angular frequency for all of points on the propagation curves. It can be seen from the two propagation curves that cut-on frequencies occur at 20Hz where the slab resonates and at 100 Hz where the rails resonate.

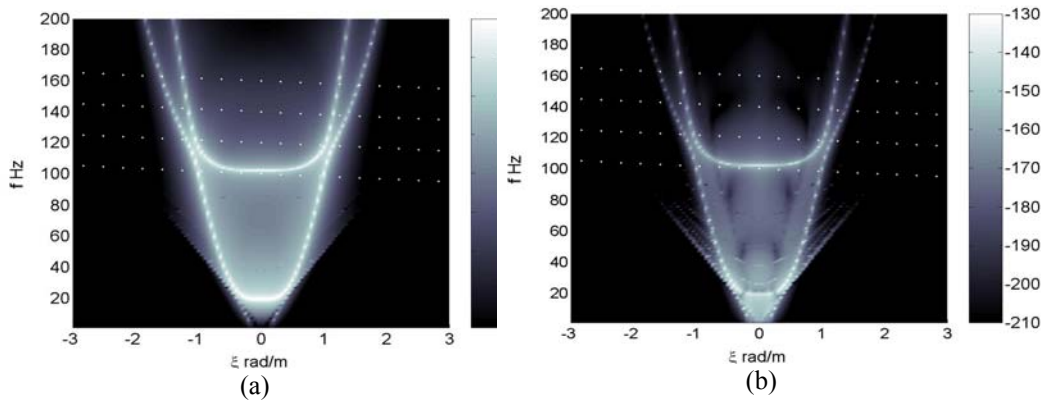


Figure 8: (a) Tangential FRF velocity ($\text{dB}_{\text{ref}} \text{ m/s/N}$) at ($r=10m, \theta=90^\circ$). (b) Radial FRF velocity ($\text{dB}_{\text{ref}} \text{ m/s/N}$) at ($r=10m, \theta=180^\circ$). Results are for a unit input at the rail and track is supported uniformly with $\phi=45^\circ, f_n=20\text{Hz}$ (No damping is included). The four parallel dotted lines give $|v_k|$ in equation (17) for excitation frequencies $\bar{f} = 100, 120, 140, \text{ and } 160\text{Hz}$.

Figure 9(a) shows the upwards mean power flow, calculated at $r_o=10\text{m}$ and integrated over a half-circle from $\theta=90^\circ$ to 270° . The four curves are for progressively-resilient slab support, *i.e.* for ∞ , 40, 20, and 5 Hz slabs. The slab is uniformly supported with $\phi=45^\circ$ as in Figure 6.c. The power results in this figure are calculated at every 1 Hz (from 1-200Hz) by averaging the results within 1Hz band (0.5 Hz on either side). In each band the results are calculated for every 0.1 Hz increment.

Averaging is used to smooth curves, which fluctuate severely otherwise. This is on account of discrete sampling of the FRFs (see Figure 4 and 8). Fluctuations are attributed to the high levels of the FRFs at points along the propagation curves. At a given excitation frequency, some values of $V(\xi_k, \omega_k)$ lie on or near the track's propagation curves, which leads to a peak. At another frequency, none of the values of $V(\xi_k, \omega_k)$ lie on or near the track's propagation curves, which leads to a trough. Introducing some damping in the track also leads to curve smoothing. This is because damping attenuates the high levels of FRF at track's propagation curves.

In Figure 9(a), the most distinguishable peaks for all curves occur at 42 Hz. This frequency is the wheel-track resonant frequency in which the wheels and axle resonate on the track. The parameters which control this peak are described in the next section. Another peak occurs at the cut-on frequency of the slab. For 40 Hz floating-slab, this happens to coincide closely with the wheel resonant frequency.

6.1 Model parameters

Parameters used for the train, track, tunnel, and soil are given below and the effect of changing certain parameters are discussed in the next sub-sections

Train: unsprung axle mass $M_a = 1000$ kg, velocity $v = 40$ km/hr, axle spacing $L=20\text{m}$.

Track: rail bending stiffness $EI_r=5\text{MPa}\cdot\text{m}^4$, rail mass $m_r=50\text{kg/m}$, slab bending stiffness $EI_s=1430\text{MPa}\cdot\text{m}^4$, slab mass $m_s=3500\text{kg/m}$, railpad stiffness $k_r=20\text{MN/m/m}$, railpad loss factor $\eta_{kr}=0.3$, slab-bearing loss factor $\eta_{ks}=0.5$, slab-bearing shear to normal stiffness ratio $\mathfrak{R}=1$ for direct fixation *i.e.* ∞ Hz and 0.5 for other slabs (*i.e.* 40, 20, and 5 Hz).

Tunnel: mean radius $r_a = 3.0\text{m}$, thickness $h=0.25\text{m}$, modulus of elasticity $E_t = 50\text{GPa}$, Poisson's ratio $\nu_t = 0.3$, density $\rho_t = 2500$ kg/m³, and no damping.

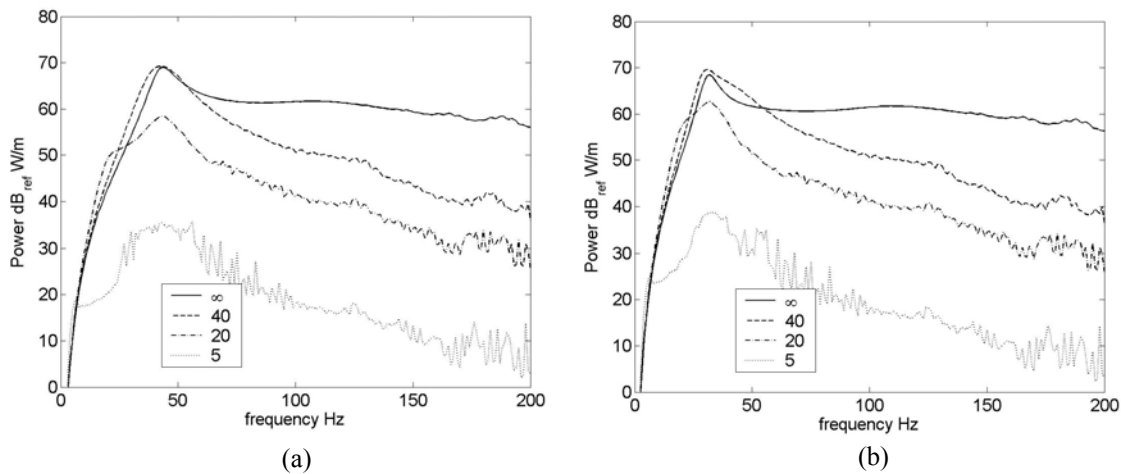


Figure 9: (a) Mean power flow radiated upwards, for different slab-bearing stiffness. (b) Effect of doubling the unsprung mass at (a).

Soil: compression wave speed $c_1 = 944$ m/s, shear wave speed $c_2 = 309$ m/s, Poisson's ratio $\nu_s = 0.44$, and no damping.

6.2 Effect of unsprung mass (wheel–track resonance)

The wheel–track system at resonance can be described as a single-degree-of-freedom system with a mass equal to the unsprung mass of the train plus that part of the rail which moves up and down with the wheel and a stiffness equal to the track stiffness underneath the wheels. A closed form equation for calculating the resonance frequency is derived from the resonance of a mass coupled to a beam on Winkler foundation and can be written as

$$(m_b \omega^2 - k_f)^3 + \frac{M_a^4}{64EI_b} \omega^8 = 0 \quad (18)$$

where m_b is the beam mass per unit length, EI_b is the beam bending stiffness, k_f is the foundation stiffness, and M_a is the coupled mass. Using the rail parameters in 6.1, the wheel–track resonance is therefore found to be 42 Hz, which matches with the results in Figure 9(a). Doubling the unsprung mass to $M_a = 2000$ kg leads to the results in Figure 9(b). Using equation 18, leads to wheel–track resonance equal to 31 Hz, which matches the results in Figure 9(b).

6.3 Effect of slab bearings

Slab bearings isolate the track from the tunnel transforming part of the wheel input into slab vibration and thus decreasing forces at the tunnel wall. For slabs with low natural frequencies, slab bearings decouple the track from the tunnel. This enables the soil FRFs to be calculated in different way. Firstly, forces on the tunnel wall can be calculated assuming a rigid tunnel. These forces can then be used as input to the tunnel–soil model to calculate the soil FRFs. Figure 11.a shows the track's propagation curves for a track on rigid foundation with infinite stiffness slab-bearings. Only one mode can propagate along rails with a cut-on frequency at 100 Hz. Introducing slab bearings (20 Hz natural frequency of slab), leads to another mode. Crossover of modes occurs between 100-120 Hz, this can be seen by comparing Figure 11 (a) and (b).

6.4 Effect of railpads stiffness

Figure 10 shows the effect of changing the railpad stiffness from 20MN/m/m to 2MN/m/m. The mean power insertion gain PFIG is used and is defined by [3]

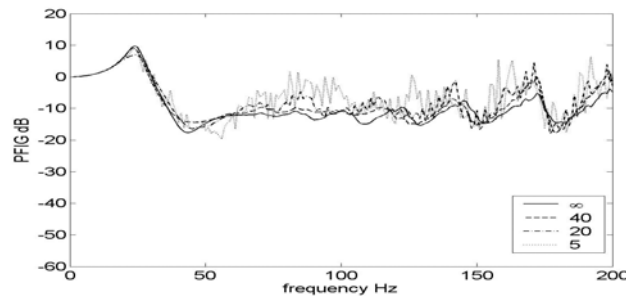


Figure 10: Insertion gain due to changing the railpad stiffness from 20MN/m/m to 2MN/m/m

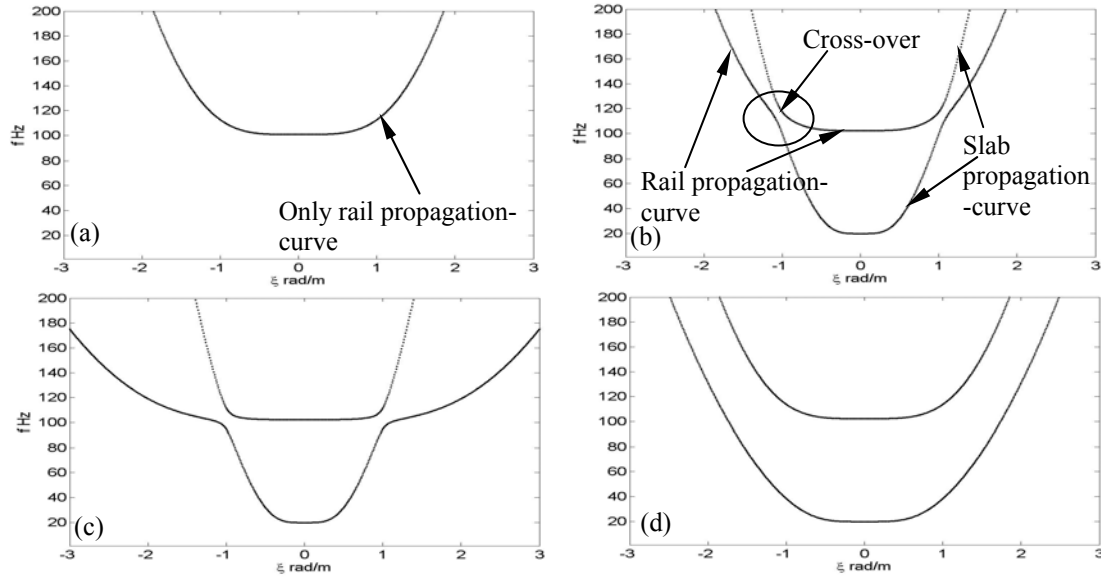


Figure 11: Propagation curves of a track (rails and slab) on rigid foundation. (a) ∞ Hz slab. (b) 20 Hz slab. (c) Same parameters as used in (b) but with 1/10 bending stiffness of rail. (d) Same parameters as used in (b) but with 1/10 bending stiffness of slab.

$$PFIG = 10 \log_{10} \left(\frac{P_{before}}{P_{after}} \right) \quad (19)$$

where P_{before} and P_{after} are the mean power radiated upwards before and after changing some of the track properties respectively. In this case for example four tracks with the same railpads stiffness (20MN/m/m) but with different slab-bearings stiffness are used. Only the railpads stiffness for all tracks are changed to (2MN/m/m). Changing the stiffness of railpad leads to a change in the wheel-track resonance frequency (from 42Hz to 24Hz) and decreases the power radiation at high frequencies (above 70Hz) by an average of 8dB.

6.5 Effect bending stiffness of rail and slab

According to equation 18, changing the bending stiffness of the rail affects the track-resonant frequency because it changes the track stiffness under the wheel. Comparing Figure 11(b) and 11(c) reveals that another effect of decreasing the rail bending-stiffness is the broadening of the rail propagation curve. The same effect can be seen for the slab propagation curve by changing the slab bending-stiffness (compare Figure 11(d) with 11(b)). Investigation of the coupled tunnel-soil model shows that it strongly attenuates large wavenumbers. This means vibration can be attenuated by broadening the track propagation curves, so that they occur at high wavenumbers and thus are attenuated by the tunnel-soil model. Figure 12(a) and 12(b) show the PFIG by decreasing the bending stiffness of the rail and the slab respectively.

6.6 Effect of distribution of slab bearings

Figure 12.c and 12.d give examples of controlling the power radiated upwards. Changing the slab-bearings distribution controls the azimuthal distribution of the load on the tunnel. In these cases the mean power flow are increased due to supporting the slab via three lines and two lines with respect to the uniform support. Further investigation is needed before a general conclusion can be made.

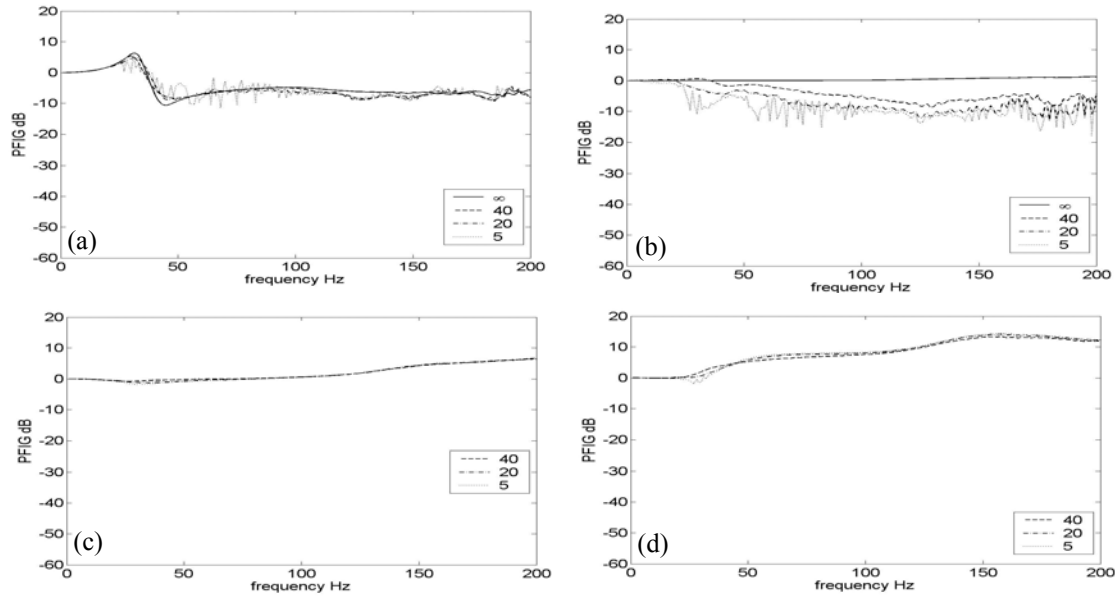


Figure 12: Insertion gain due to (a) changing the bending stiffness of rail from $5\text{MPa}\cdot\text{m}^4$ to $0.5\text{MPa}\cdot\text{m}^4$. (b) changing the bending stiffness of slab from $1430\text{MPa}\cdot\text{m}^4$ to $143\text{MPa}\cdot\text{m}^4$. (c) Replacing the uniform slab bearings by three lines of slab bearing ($\psi=45^\circ$). (d) Replacing the uniform slab bearings by two lines of slab bearing ($\Omega=45^\circ$).

Conclusions

A new method based on power flow calculations is presented to evaluate the performance of vibration countermeasures for underground tunnels. An expression of the power radiation is derived for an infinite train moving through the tunnel. A three-dimensional model of a track coupled to a tunnel in the ground is used to investigate the upward mean power from the tunnel. The track properties along with the tunnel–soil–track interaction play important roles in controlling the radiated power. The method is used to investigate the effect of unsprung mass, railpads, slab bearings, railpads, and bending stiffness of rail and slab.

Acknowledgement

The authors would like to thank Cambridge Overseas Trust COT and London Underground Limited LUL for their support of this project.

References

- [1] D.E. Newland, *An introduction to Random Vibrations. Spectral & Wavelet Analysis*. Longman Singapore Publishers Ltd, 1975.
- [2] J.A. Forrest, *Modelling of Ground Vibration from Underground Railways*. PhD dissertation, Cambridge University, 1999.
- [3] J.P. Talbot, H.E. Hunt, On the performance of base-isolated buildings, *Building Acoustics*, 7(2), 163-178. 2000.